PREDICTIONS OF RADIATIVE AND CONVECTIVE FLUXES AT STAGNATION POINT FOR AN EARTH HIGH-SPEED RE-ENTRY

Franck Mazoué (1), Philippe Reynier (1)

(1) *Ingénierie et Systèmes Avancés, Pessac, France,*
Email : franck.mazoue@isa-space.eu
Email: Philippe.Reynier@isa-space.eu

ABSTRACT

Planetary entries are often characterized by strong radiation and ablation effects. This is particularly the case for sample return missions. Here in order to improve the state-of-the-art for such projects, computations are performed accounting for radiation and ablation. The main objective is to evaluate the blocking effect induced by the blowing of pyrolysis gases on the heat –flux and on the shock layer.

1. INTRODUCTION

In the frame of its activities, ISA has started a study for evaluating the convective and radiative blockages for Earth high-speed re-entry. A past review [1] on convective blockage has shown that in despite of many numerical, experimental and flight data related to this problem, no extensive investigation focusing only on this topic was undertaken for many years. This review seems to have been the first effort to gather the sparse data available on convective blockage in relation with Earth high-speed entry. This review was not limited to the numerical and CFD results but the different engineering models to predict the blocking factor, that are based on a certain level of empiricism, was also analyzed and the modelling that seemed to be the most valuable was selected. However, there is a lack of reliability of engineering correlations for blockage factor since these correlations have a high level of empiricism.

Results obtained for high speed Earth re-entries showed the strong impact of the blowing of the pyrolysis gases on convective and radiative heat-fluxes. CFD results [2-3] obtained in the frame of the Stardust project exhibited a reduction of the total heat-flux around 35% at the stagnation point for peak heating conditions. Ablation has other consequences. It reduces the surface gradients of temperature and that of various species mass fractions, causing a decrease of convective and diffusive heat-fluxes. CO, one of the main ablation products (for carbon based materials), lowers significantly the wall enthalpy. There is a slight increase of radiation with ablation before the peak heating [3]. Usually there is a deeper penetration of the shock layer by the ablation species C and CO in the earlier time of the trajectory as reported in [2,4], and the increase in radiation from C lines and CO(4+) is only partially offset by the absorption of ablation species during that period.

Table 1: Maximum heat fluxes for EVD mission [5]

Trajectory	Convective flux MW/m^2	Radiative flux MW/m^2	Total flux MW/m^2	Total Heat load MJ/m^2
E1	11.5	7.5	18.8	106.9
E2	15.7	18.1	33.8	178.3
E3	9.35	4.55	13.9	243.2
E4	7	1.9	8.9	154.6

Radiation is a very complex phenomenon since it is strongly influenced by ablation. This phenomenon is a key issue for Earth high speed re-entry since it has a significant contribution to the total heat-flux as shown in Table 1. The presence of absorbing species produced by the pyrolysis process or present in the shock layer (this depends on atmosphere composition) can involve strong variations of the heat-flux level. According to Park [6], at the peak heating point of Apollo 4 entry trajectory, the convective and radiative heating rates were about 3.5 and 1.7 MW/m^2 at the stagnation point. However, about 2/3 of the convective heating rate was due to absorption of radiation in the boundary layer. The intrinsic components of convective and radiative heating rates were about 1.1 and 4.1 MW/m^2 respectively. More recently the numerical results obtained during the Huygens project [7-8] have demonstrated the strong decrease of radiative and convective heat-fluxes as well as the change of flow topology (shock stand-off distance) for coupled radiation/flow-field calculations against non coupled simulations. These results highlighted also a strong decrease of radiative heat-flux when absorption was accounted for.

In the frame of the current effort and in the perspective of assessing the reliability of engineering correlations for convective blockage with numerical results, a first study has been started to evaluate the convective blockage using numerical simulations. In this objective, numerical simulations have been undertaken for a superorbital re-entry capsule and a carbon phenolic thermal protection system. The calculations have been carried out with and without ablation. Then the results have been post processed with a radiation solver to estimate the radiative heat-flux with and without ablation.

2. CONTEXT

Some years ago, ESA studied the scenario for a sample return mission to Mercury [9]. This mission would consist in a single ARIANE 5 rocket launch, and then the probe will fly to Mercury. Since Mercury has no atmosphere, engines will be used to ensure the landing. Then a capsule, containing the samples will be launched for the return flight to Earth. Concerning aerothermodynamics, the main issue of such a mission is the re-entry in Earth atmosphere of the small capsule bringing back the samples. The capsule has a weight of 20 kg and the nose radius is 0.4 m. With such constraints, an accurate prediction of the heat flux at the capsule nose during the entry is required to design the thermal protection system. Preliminary assessment [10] was performed using Navier-Stokes calculations and a sensitivity analysis to the modelling (non equilibrium, frozen flow, equilibrium) was also carried out. In this previous investigation, no radiation calculation was performed. These first predictions showed that 1/3 of the thermal shield mass [9] would be lost during an Earth entry.

Here, the flow around the same capsule will be computed with and without ablation. Two different cases are performed with ablation. In the first one the blowing of the pyrolysis products is accounted for while in the second only surface reactions related to sublimation and oxidation are considered. Then the results will be processed using a radiation tool to compute the radiative heat-flux over the heat-shield.

Table 2: Upstream flow conditions for the numerical simulations of Earth entry

Velocity (km/s)	14.17
Pressure (Pa)	8.7
Density (kg/m^3)	1.32 10^{-5}
Temperature (K)	185

3. CFD CALCULATIONS

3.1. Modelling with TINA

TINA [11] is a Navier-Stokes solver, accounting for chemical and vibrational non-equilibrium. It is adapted to the simulation of hypersonic flows encountered in high enthalpy nozzles or during entries, where enthalpies and local Mach numbers are high enough to allow non-equilibrium effects. The solver uses a time marching algorithm with the approximate Roe-Riemann solver and the flux limiters proposed by Yee [12] for inviscid flows. The thermo-chemistry is implicitly coupled to the flow-field for computing the non-equilibrium effects. The tool can be coupled with PARADE [13] with a one dimensional coupling to compute the radiative heat-flux over the surface.

The atmosphere around a capsule has been computed using the two thermochemical models proposed by Dunn & Kang [14] and Park et al [15]. Both models account for 11 species (O_2, NO, N_2, O, N, O^+, O_2^+, NO^+, N^+ N_2^+, e^-) and 16 reactions. Since an ablative TPS is considered, the products produced by the resin pyrolysis has to be considered. TPS material is supposed to be the carbon phenolic FM5055 [16-17] which is well documented in the literature. The additional elements present in the shock-layer are modelled as in [18] with 11 additional species: C, C_2, C_3, CO, CO_2, H, C_2H_2, H_2, HCN, C_2H and CN. This means also 21 additional chemical reactions.

Ablation products are considered through a blowing file providing pyrolysis gas mass flow rate and species mass fraction at the ablative boundary. An alternative to take into account ablation is the modelling of oxidation and sublimation of the TPS material without considering the blowing of the pyrolysis gases. Oxidation and sublimation occur for temperatures higher than 1 000 K and 3 000 K respectively. These two processes can be modelled as proposed by Park [19] with three equations between solid carbon and the oxygen and three other equations for sublimation (producing C, C_2 and C_3).

For the calculations an isothermal wall at 3 000 K was considered.

Table 3: Cases computed with thermochemical model and ablative condition

Case	Model	Ablative
1	Park et al	No
2	Dunn & Kang	No
3	Park et al	Blowing
4	Park et al	Surface reactions

3.2. Non ablative results

The computations have been performed using TINA for the trajectory point reported in Table 2. A mesh with 60×80 cells (see Figure 1) has been used for the computations. First cell along the axis was 10 µm, this is very small but needed for accounting for an ablative boundary. Different calculations have been carried out with the two different thermochemical models and ablative conditions. They are reported in Table 3. For the non ablative case calculations have been converged in less than 100 000 iterations with a residual of the order of 10^{-6}. The ablative cases have been initialized with non ablative results and convergence was obtained in 80 000 iterations with a residual in the range of 10^{-4}. CFL numbers used for the calculations were in between 1 and 5 for non ablative calculations and 0.1 and 0.2 for the ablative cases.

Figure 1: Mesh used for the calculations

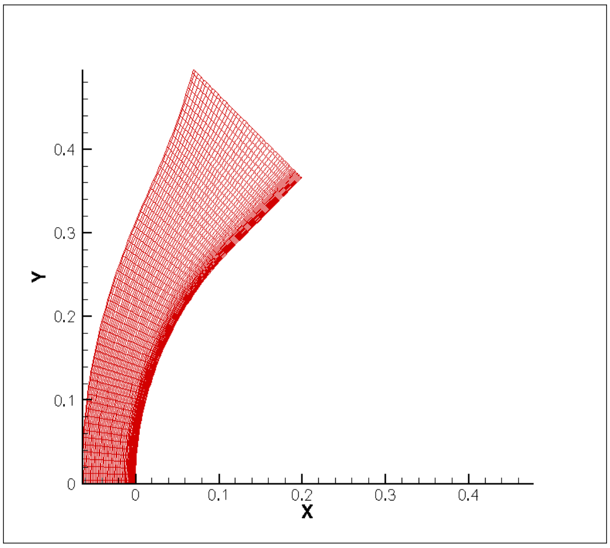

Figure 2: Electron mass fraction for Case 2

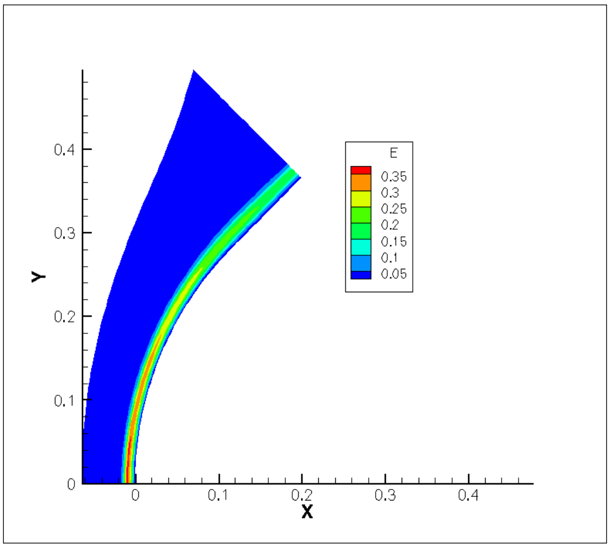

First Cases 1 and 2 from Table 3 have been computed to assess the result sensitivity to the thermochemical model. The thermochemistry model has a high influence for the assessment of ionisation and heat-flux. This is clearly highlighted in Figures 2 and 3. The flow-field distributions show that the mass fraction of electron predicted by the model of Dunn & Kang [14] (see Figure 2) is twice the level predicted by the mode of Park et al [15] (see Figure 3). Additionally the shock stand-off in the stagnation region is a little bit smaller with the first model. The differences in the chemistry of the shock-layer lead to different predictions of the wall heat-fluxes as shown in Figure 4 where the wall heat-fluxes, predicted using both models, are plotted. At the stagnation point the heat-flux predicted with the Park et al model is 33 % higher than the one predicted with Dunn & Kang's model. This is due to the difference in the shock layer topology and thermochemistry however due to the lack of valuable experimental data for comparisons and assessment of the thermochemical model reliability it is difficult to select the best model. Hence, for the predictions accounting for ablation the model of Park et al has been retained but there is no argument to select one model or another.

Figure 3: Electron mass fraction for Case1

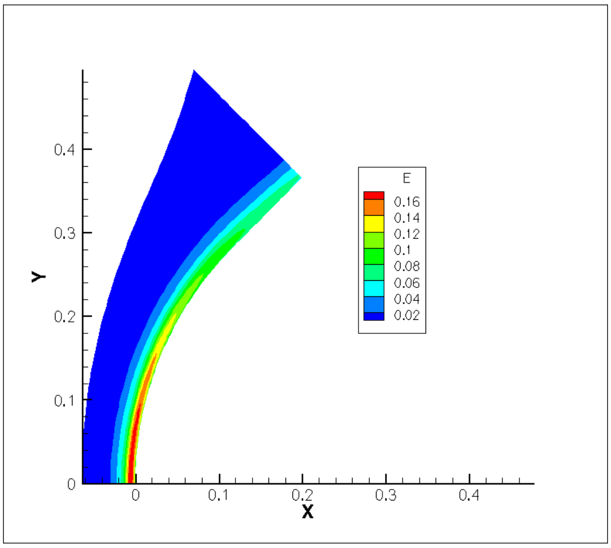

Figure 4: Heat-flux predicted for Cases 1 and 2

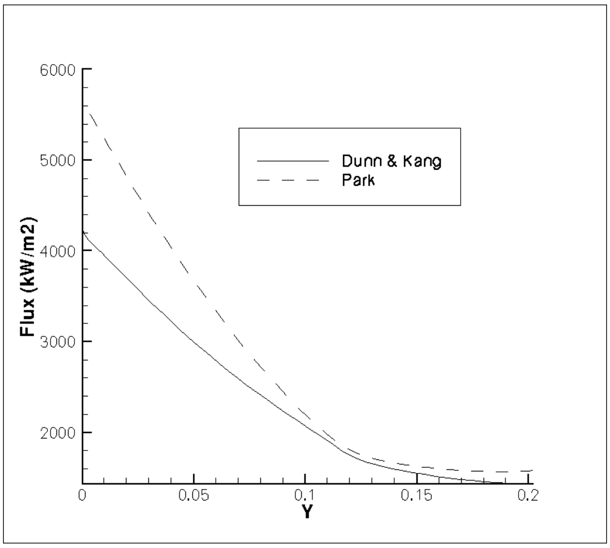

Figure 5: Distribution of vibrational temperature for Case 1

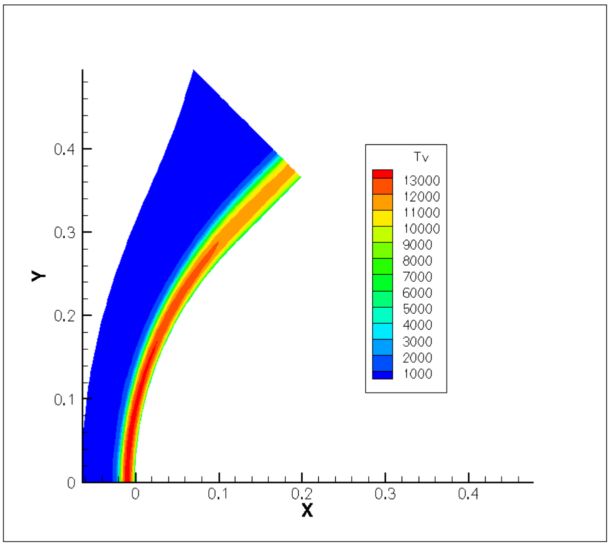

Figure 6: Distribution of vibrational temperature for Case 3

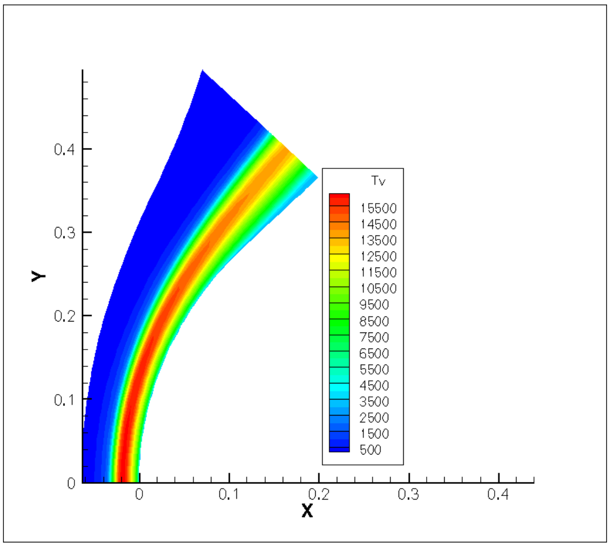

3.3. Ablative results

The Cases 3 and 4 of Table 3 have been computed and initialized with the results obtained for the Case 1. The results were converged in 70 000 more iterations with a residual of 10^{-3}. The comparisons between the results of Cases 1 and 3 highlight the strong impact of the blowing on the shock layer. The distributions of the vibrational temperature are plotted in Figures 5 and 6. The impact of blowing on the shock-layer is easy to see in Figure 6. The shock stand-off at the stagnation point has increased from 4 to 5 cm due to the penetration of the pyrolysis gas in the shock-layer. The blowing has also a strong effect at the leading edge (see Figure 6). Here, it might be overestimated and further effort would be needed to clarify this point. From the flow-field computations, parameters such as temperatures (T_t, T_v), density and molar fractions have been extracted along the stagnation line, first for comparisons and finally for the radiation computations. The distributions of the vibrational (dashed line) and translational (continuous line) temperatures along the axis and at the leading edge are plotted in Figures 7 and 8 respectively. High temperatures are reached at the shock position; more than 26 900 K with and without ablation. In both cases, the thermal non-equilibrium region is relatively large (more than 1cm) with a level of vibrational temperatures around 16 000 K. Figure 8 presents the temperature evolution at the leading edge. The x axis corresponds to the distance (in meter) perpendicular to the normal of the surface. The thickness of the shock layer at the leading edge and the stagnation point is relatively the same (0.4cm for the case without ablation and 0.5cm for the case with ablation) whereas the non-equilibrium region is smaller (2.5 cm compare to 3.3 cm previously).

Figure 7: Temperature distributions along the stagnation line

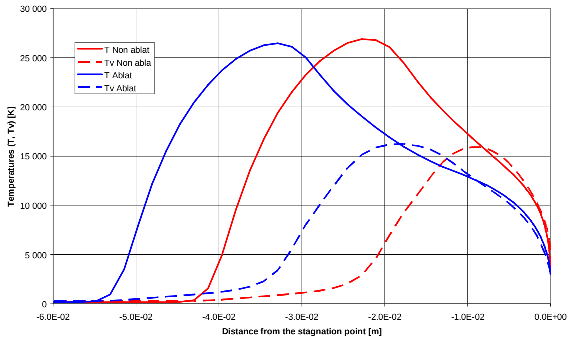

Figure 8: Temperature distributions along the leading edge

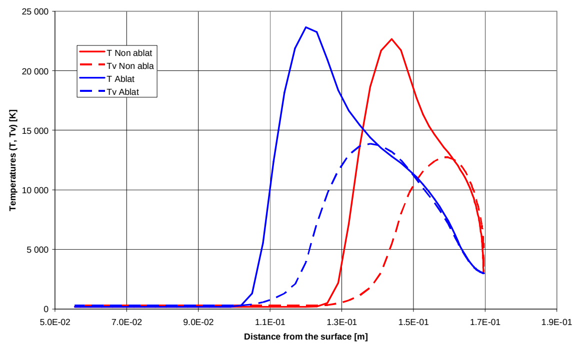

In Figures 9 and 10 the mass fraction of the neutral, ionized and ablation species along the stagnation line are presented respectively. In the shock layer, N_2 and O_2 are completely dissociated and the level of NO is very low. Concerning the ionic species, there are substantial levels of O^+ and N^+ while very low mass fractions (not shown here) of N_2^+, O_2^+ and NO^+. In fact crossing the shock O_2 is rapidly and highly dissociated to form O and O^+. Small amount O_2^+ is observed but can be neglected for the radiation computations. N_2 is dissociated to form N and NO by recombination with O but a small fraction of NO is created. A large part of the atomic nitrogen produced by the dissociation of N_2 is ionized in N^+ as shown in Figure 10. The highest species concentrations coming from the atmosphere are for N_2, N, N^+, O, and O^+. The other species concentrations are lower by at least a factor 10.

Figure 9: Neutral species

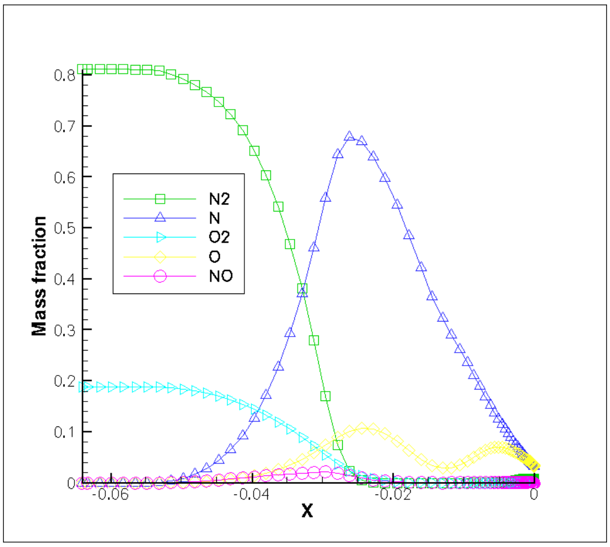

Figure 10: Ionized and ablation species

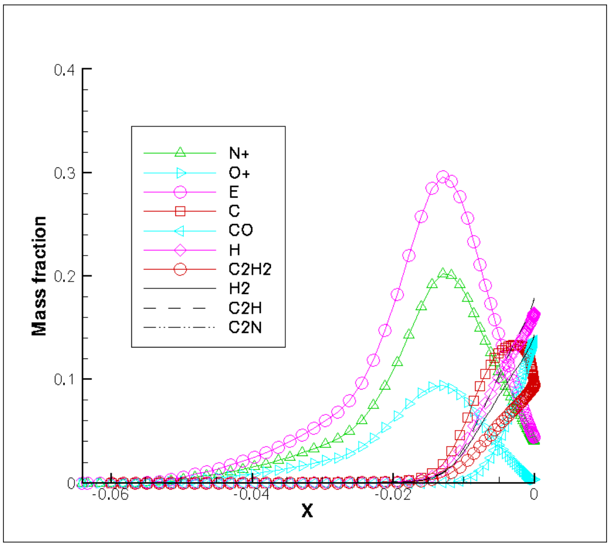

The species produced by the blowing in the shock-layer are plotted in Figure 10. Among these species, C, CO, H, C_2H, C_2N, C_2H_2 and H_2 reach a subsequent level in the shock layer in the stagnation point region. From the plot of the flow-field distribution of the mass fraction of C2 and C3 showed respectively in Figures 11 and 12 it is clear that the stagnation region is not representative of the whole shock-layer. In the region near the leading edge due to lower temperature levels, the ablation products are far to negligible. This is an important point since species such as C_2, C_3 and also CO has strong radiative properties. C_2 and C_3 possess absorption properties while CO is a strong radiator.

Figure 11: Mass fraction of C_2

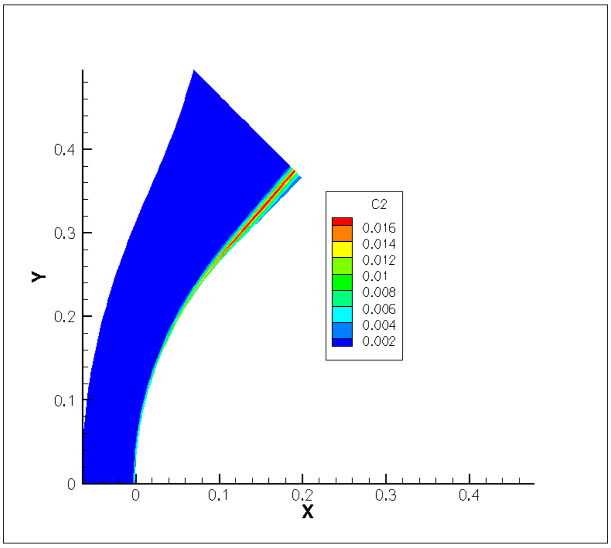

Figure 12: Mass fraction of C_3

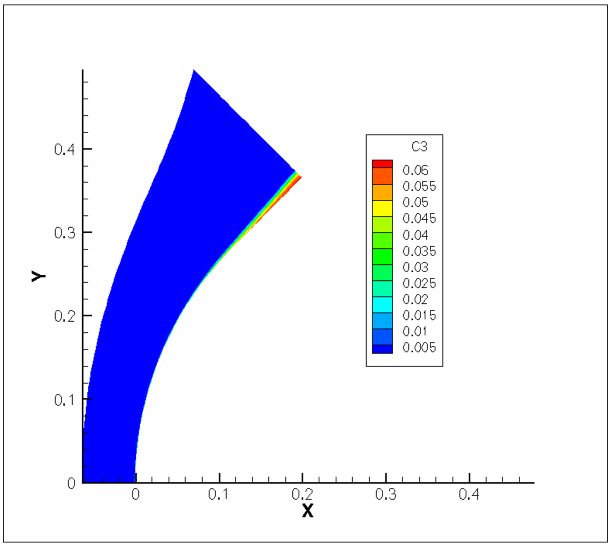

Now, if we look at the wall heat-flux the influence of ablation on the convective heat-flux can be assessed using the results obtained for Cases 3 and 4 of Table 3. The distribution of the heat-flux along the wall is plotted in Figure 13. The computations accounting for ablation highlight the effect of this phenomenon on the heat-flux level. The calculations with the blowing effect predict a heat-flux which is 71% lower than the one predicted without ablation. The numerical simulation performed without blowing but accounting for surface reactions due to oxidation and sublimation predicts a heat-flux level in between that is 18% lower than the non ablative flux. This simulation does not consider nitridation which might play a significant role producing some CN in the shock layer that is a strong radiator. As a consequence this last computed case might underestimate the ablation effects. Concerning the results obtained with the blowing, the ablation effect is very high. This might be the consequence of an overestimation of the blowing in this study more efforts will be needed to confirm this point.

Figure 13: Wall convective heat-flux distributions for Cases 1, 3 and 4

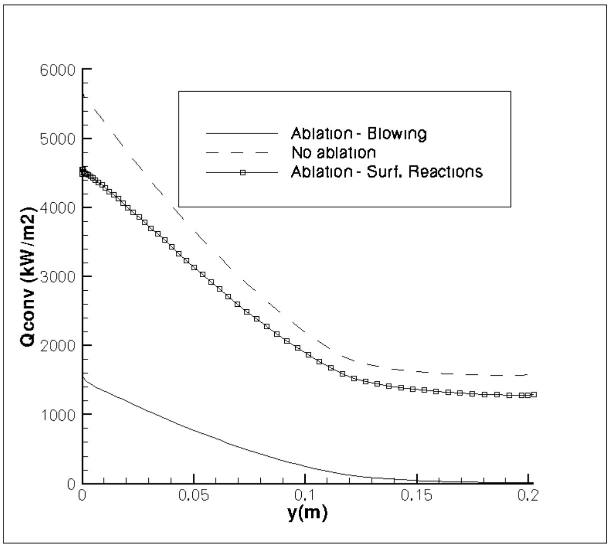

4. RADIATION ANALYSIS

4.1. Approach

With the density, the molar fractions and the two temperatures (translational and vibrational), the radiation heat flux has been computed with PARADE [13]. PARADE code has been developed in collaboration between Fluid Gravity Engineering Ltd (UK) and the Institute of Raumfahrtsysteme from Stuttgart (D) under an ESA/ESTEC contract in 1996 for air species first. Since then, it has been modified in order to take into account more species, in particular CN for supporting the Huygens project. The code is used to compute flow-field emission and absorption, between the shock layer and the surface of the probe.

The spectral emission and absorption are determined as function of transition level (from upper level to lower level) and emitting population of this level. The population can be derived from the Quasi-Steady-State (QSS) method or by a Boltzmann method in order to take into account the non-equilibrium or equilibrium regime respectively.

The radiative computations have been performed with the Boltzmann assumption for the determination of the population of the excited molecular states.

The species taken into account for an EVD high-speed entry into Earth atmosphere are N_2 (1+, 2+ and bh2), N_2^+ (1-), N, N^+, O, O^+, O_2 and NO. O_2^+ and NO^+ have been disregarded in both cases (with and without ablation) for the radiation computation for two reasons: first the spectroscopic data were not available in the present version of PARADE and secondly these molecules have not been yet implemented in PARADE.

For the same reason, the ablation products taken into account for the radiation computations were CN (red and violet bands), C_2 (Swan) and C and H atoms. C_3 cannot be accounted yet with PARADE. There is little experimental data on this molecule (and also for C_2) and most of it dates back to the Galileo project. Moreover, the radiation modelling of a triatomic species like C_3 (one of the main ablation products for a carbon phenolic TPS) is difficult and will represent a strong effort from a computational point of view.

4.2. Radiative heat flux

For this study, radiative emission has been calculated using PARADE at the stagnation point and near the leading edge of the capsule. No full coupled computations were undertaken since they represent a very prohibitive computational effort.

Self-absorption by molecules was taken into account for the analysis over the wavelength range (200 nm – 4 000 nm). At first, the result dependence on the discretisation has been verified. Several calculations using 20 000, 100 000 and 500 000 points over the wavelength range have been carried out at the stagnation point of the ablative case. The results are reported in , they demonstrate that a number of points of 100 000 is sufficient to model correctly the wavelength range. This agrees with previous results obtained during the Huygens project [7-8].

presents the radiative heat fluxes in both cases (with and without ablation) at the stagnation point and the leading edge. They have been predicted for the Cases 1 and 3 of Table 3.

Table 4: Influence of the wavelength discretisation for Case 3 at stagnation point

Number of points	20000	100000	500000
Radiative heat-flux (kW/m^2)	485	483	483

Table 5: Radiative heat fluxes for Cases 1 and 3

Case	Stagnation point	Leading Edge
Non-ablative	339 kW/m^2	76.36 kW/m^2
Ablative	443 kW/m^2	201.7 kW/m^2

The levels at the stagnation points are 443 and 339 kW/m^2 for the cases with and without ablation products respectively. These levels are low due to the trajectory point taken for the numerical simulations. At peak heat flux, the level of the radiative flux might be of the same order of magnitude than the convective heat flux. Indeed, the entry conditions of the computed point reported in Table 2 correspond to an altitude of 80 km. This is to say earlier than the peak heat flux point along the trajectory. In fact the high altitude of the calculated point explains at least partially the results obtained for the blowing case. Since, the blowing is strong at the beginning of the ablation regime it is there more efficient and the blocking effect high. The blockage depends also on the ratio between the mass flow rates of gases crossing the shock layer (from upstream) and those blown by the TPS pyrolysis. The difference in the heat fluxes calculated at the stagnation point without and with ablation products is due to the radiation of the CN molecules for the ablative cases. The fact that the computed point is at high altitude explains the increase of radiative heat-flux when accounting for ablation. Such a slight increase of radiation, when accounting for ablation before the peak heating, was also noted for the Stardust project [3]. This increase is due to deeper penetration in the shock-layer of species such as C, CN and CO in the earlier time of the trajectory. Even if absorption is taken into account its effect offsets on partially the increase in radiation from C lines and CO(4+) [2,20].

At the leading edge the level of radiative flux is very lower for both calculations. But the same trend is observed with a higher radiative heat-flux when ablation is taken into account. Since the mass fraction of C_2 and C_3 are high along the flank of the capsule as shown in Figures 11 and 12 the absorption should be however high in this region and as consequence the radiative flux even lower than the one computed but C_3 absorption was not accounted for in this study.

5. CONCLUSIONS

In this study, a first effort has been carried out to assess the ablation effects on heat-flux for Earth high-speed re-entry conditions. The computed case is at high altitude to have radiative and convective heat-fluxes of the same order. The trajectory point is just at the beginning of the radiative pulse. As a consequence the case is not the best one to check the existing correlations predicting radiative and convective blocking factors. And other entry conditions with an available complete trajectory will have to be used for further activity in this direction.

Beside this problem, the numerical simulations have shown the maturity of the available tools to assess radiative and convective heat-fluxes for Earth EVD re-entry. The consideration of phenomena such as ablation and radiation show a strong impact on the heat-flux levels and this will have some consequences when designing heat-shields for sample return missions. For these missions the mass constraint is high and the optimization of the heat-shield will be a key issue.

The next steps to continue this effort will be to compute EVD entry conditions for radiative and convective peak heating and to account for absorption. Further work will be needed to achieve fully coupled CFD/radiation calculations or/and to account for absorption from ablative species such as C_3.

REFERENCES

[1] Reynier, Ph., Convective blockage during Earth re-entry: A review, AIAA Paper 2008-3806, 40th Thermophysics Conference, Seattle, 23-26 June, 2008.

[2] Olynick, D., Chen, Y.-K., and Tauber, M. E., Aerothermodynamics of the Stardust sample return capsule, Journal of Spacecraft and Rockets, Vol. 36, pp. 422-462, 1999.

[3] Gupta, R. N., Aerothermodynamic analysis of Stardust sample return capsule with coupled radiation and ablation, AIAA Paper 99-0227, 1999.

[4] Moss, J. N., Anderson, E. C., and Bolz, C. W., Aerothermal Environment for Jupiter Entry Probes, AIAA Paper 76-469, 11th Thermophysics Conference, SanDiego, CA, June 1974.

[5] CDF study report, MSR Mars Sample Return: The Second Aurora Flagship Mission, Report CDF-16(A), 2003.

[6] Park, C., Stagnation point radiation for Apollo 4, Journal of Thermophysics and Heat Transfer, Vol. 18(3), pp. 349-357, 2004

[7] Mazoué, F. and Marraffa, L., Flow-field/Radiation coupling analysis for Huygens probe entry into Titan atmosphere AIAA Paper 2005-5392, 2005.

[8] Mazoué, F., Graciano, J., Tournebize, L., and Marraffa, L., Updated analysis of the radiative heat flux during the entry of the Huygens probe in the Titan atmosphere ESA SP-563, 5th European Symposium on Aerothermodynamics for Space Vehicles, Cologne, November 2004

[9] Scoon G., Lebreton J.-P. and Coradini M., *Mercury Sample Return*, ESA Assessment Study Report, SCI(99)1, Nov., 1999.

[10] Reynier Ph., Marieu V. and Marraffa L., "Aerothermodynamics Developments for Planetary Missions", In Proceedings of the 1st Joint French-German Symposium on Simulation of Atmospheric Entries by Means of Ground Test Facilities, SSAE 99, pp. 2.5.1-2.5.8, Stuttgart, Nov. 17-19, 1999.

[11] Tina Version 4: Theory and User Manual, Fluid Gravity Engineering, TN 89/96 Issue 7, Lyphook, United-Kigdown, March 2008.

[12] Yee, H. C., Construction of explicit and implicit symmetric TVD schemes and their applications, Journal Comp. Phys, Vol. 68, pp. 151-179, 1987.

[13] Smith A.J., Gogel T., Vandevelde P. and Marraffa L., PlasmA Radiation DatabasE, final report ESTEC contract 11148/94/NL/FG, April 1996

[14] Dunn, M. C., and Kang, S. W., Theoretical and experimental studies of re-entry plasmas, NASA CR-2232, 1973.

[15] Park, C., Jaffe, R. L., and Partridge, H., Chemical-kinetics parameters of hyperbolic Earth entry, Journal of Thermophysics and Heat Transfer, Vol. 15(1), pp. 76-90, Jan.-March 2001.

[16] Milos, F. S., Chen, Y.-K., Squire, T. H., and Brewer, R. A., Analysis of Galileo probe heat-shield ablation and temperature data, Journal of Spacecraft & Rockets, Vol. 36(3), pp. 298-306, 1999.

[17] Ahn, H.-K., Park, C., and Sawada, K., Response of heatshield material at stagnation point of Pioneer-Venus probes, Journal of Thermophysics and Heat Transfer, Vol. 16(3), pp. , 2002.

[18] Roberts, T. P., Modelling gas/surface interaction processes of ablating wall boundaries associated with planetary entry, 2th European Symposium on Aerothermodynamics for Space Vehicles, ESTEC, ESA SP-367, Feb. 1995.

[19] Park, C., Effects of atomic oxygen on graphite ablation, AIAA Journal, Vol. 14(1), pp. 1640-1642, Sept. 1996.

[20] Moss, J. N., Anderson, E. C., and Bolz, C. W., Viscous shock-layer solutions with radiation and ablation injection for Jovian entry, AIAA Paper 75-671, AIAA 10th Thermophysics Conference, Denver, CO, May 1975.